



# Pd Nanoparticles Assembled on Metalporphyrin-Based Microporous Organic Polymer as Efficient Catalyst for Tandem Dehydrogenation of Ammonia Borane and Hydrogenation of Nitro Compounds

Zhijuan Zou<sup>1</sup> · Yaya Jiang<sup>1</sup> · Kunpeng Song<sup>1,2</sup>

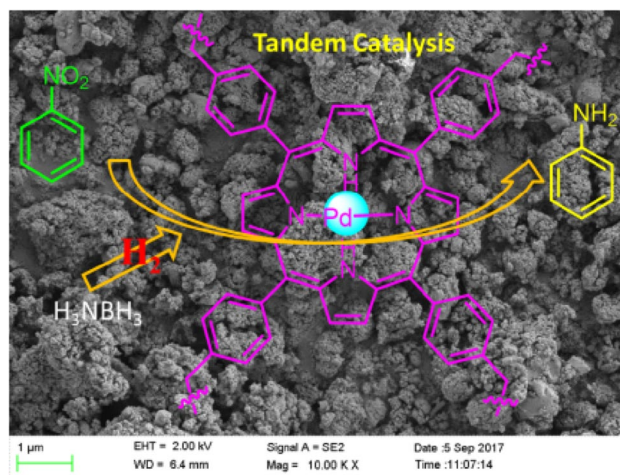
Received: 12 July 2019 / Accepted: 6 November 2019 / Published online: 14 November 2019  
© Springer Science+Business Media, LLC, part of Springer Nature 2019

## Abstract

Metalporphyrin-based porous polymers supporting high dispersed Pd nanoparticle (NP) catalysts (HUST-1-Pd) were prepared with a novel solvent-knitting hyper-crosslinked polymer method using 5-, 10-, 15-, and 20-tetraphenylporphyrin (TPP) as building blocks. The N<sub>2</sub> sorption isotherms of the catalysts show that the HUST-1-Pd possesses many ultra-micropores and continuous mesopores. The NPs are assembled on tetraphenylporphyrin structures and show Pd-N<sub>4</sub> composition-dependent catalysis for methanolysis of ammonia borane (AB) and hydrogenation of aromatic nitro compounds to primary amines in methanol solutions at room temperature. The nano-palladium reduced by NaBH<sub>4</sub> has efficient catalytic activity for AB methanolysis. A variety of R-NO<sub>2</sub> derivatives were reduced selectively into R-NH<sub>2</sub> via palladium catalyzed tandem reactions with 5–30 min of reaction time with conversion yields reaching up to 90%. The derivatives also give excellent recycling performance (more than 10 times). Furthermore, the turnover frequency (TOF) can reach 87,209 h<sup>-1</sup>. The HUST-1-Pd compounds represent a unique metal catalyst for hydrogenation reactions in a green environment without using pure hydrogen.

## Graphic Abstract

A monodisperse Pd NPs embed in porphyrin-based microporous organic polymer was reported to catalyse the tandem dehydrogenation of ammonia borane and hydrogenation of R-NO<sub>2</sub> to R-NH<sub>2</sub> at room temperature. The catalyst is efficient and reusable in an environment-friendly process with short reaction times and high yields.



Zhijuan Zou and Yaya Jiang contributed equally to the paper.

**Electronic supplementary material** The online version of this article (<https://doi.org/10.1007/s10562-019-03028-7>) contains supplementary material, which is available to authorized users.

Extended author information available on the last page of the article

**Keywords** Microporous organic polymer · Metalloporphyrin · Tandem reaction · Hydrogenation

## 1 Introduction

Aniline and its derivatives are important raw chemical materials with more than 4,000,000 tons produced every year [1]. They are used widely for the synthesis of dyes, polymers, agrochemicals, pharmaceuticals, and various fine chemicals [2, 3]. One common route for their preparation is the reduction of their corresponding nitro derivatives in a hydrogen atmosphere [4, 5]. However, hydrogen is hardly dissolvable in a nitro compound solution and is dangerous for transport. The need for an easily transportable source of hydrogen has attracted considerable attention in the context of novel environmentally benign energy sources. We hypothesize that an opportunity exists to empty a “hydrogen storage materials” as a readily available hydrogen source [6]. In this context and in efforts to look ahead for alternatives to petroleum-based fuels, ammonia borane ( $\text{H}_3\text{N-BH}_3$ , AB) appears attractive in view of its high thermal stability and hydrogen content (19.6% by weight) [7]. Recent reports have focused on several aspects of AB as a hydrogen source and the means to control its  $\text{H}_2$  release [8]. A large number of studies have reported applications of AB in hydrogenation reactions catalyzed by heterogeneous metal support porous materials like zeolites [9, 10], porous carbon [11], and metal–organic frameworks (MOFs) [12–14]. Experimental investigations have demonstrated that hydrogenation of porous catalytic materials is affected by their  $\text{H}_2$  capture capacity with the reason being that low  $\text{H}_2$  capture capacity of porous materials decreases the  $\text{H}_2$  concentrations near the catalytic sites’ hydrogenation performance [15–17]. Therefore, there is still a great need to search for new types of heterogeneous catalysts that possess a high  $\text{H}_2$  adsorption capacity to efficiently ensure hydrogenation under ambient conditions.

To improve the  $\text{H}_2$  adsorption capacity of porous materials, several strategies can be used, such as increasing surface area, tuning pore size, and introducing  $\text{H}_2$ -philic active sites [18] such as heteroatoms, metal ions and functional groups. Distinguished from other porous materials such as zeolites, porous carbon, and MOFs, the inherent structural features of MOPs show that they are composed of pure organic elements that endow them with high chemical stability, adjustable compositions, and synthetic diversity, which make them more competitive in optimizing  $\text{H}_2$  adsorption capacity for hydrogenation of nitro compounds. Over the past decade, numerous MOP materials acting as heterogeneous hydrogenation catalyst have been developed [19–21]. However, only a few MOPs with high  $\text{H}_2$  capture have been reported thus far [22, 23]. Therefore, the development of novel MOP

materials with a high  $\text{H}_2$  capacity as a heterogeneous catalyst for efficient hydrogenation under ambient conditions is still highly desired.

Porphyrins are ideal building blocks of porous materials containing nitrogen atoms and a large  $\pi$ -conjugated system that not only enhances their interactions with  $\text{H}_2$ , but also aid in metal ion complexation, demonstrating their potential applications in gas storage and heterogeneous catalysis [24]. Palladium-based catalysts have been shown to facilitate the dehydrogenation of AB and selectively hydrogenate a variety of substrates. Therefore, a catalytic tandem reaction in which Pd serves a dual role to catalyze the dehydrogenation of AB while hydrogenating  $\text{R-NO}_2$  would be an efficient way to generate  $\text{R-NH}_2$ . Meanwhile, the Pd-porphyrin complexes have been proven to be a series of homogenous catalysts in hydrogenation reactions [25, 26]. Recently, we found a simple and low-cost solvent-knitting hyper-crosslinked polymer method that can knit aromatic compounds to obtain ultra-microporous networks and obviously improve the metal dispersion of knitting materials [27]. Taking these advantages into account, the HUST-1 with ultra-micropores and catalytic activity sites was successfully knitted by using dichloromethane as the external crosslinker and 5-, 10-, 15-, and 20-tetraphenylporphyrin as building blocks under  $\text{AlCl}_3$  catalysis [28]. After incorporating Pd into the centered square-planar coordination site of porphyrin, the catalyst HUST-1-Pd not only possesses high dispersity of Pd nano particles, but also shows excellent catalytic efficiency for hydrogenation of nitro compounds in the presence of AB and  $\text{NaBH}_4$ . What is more, the catalyst system holds high recycling potential at room temperature and atmospheric pressure.

## 2 Results and Discussion

The chemical structures of HUST-1 were confirmed by Fourier transform infrared (FTIR) spectroscopy and solid-state  $^{13}\text{C}$  cross-polarization magic-angle spinning (CP-MAS) NMR (Supporting Information, Fig. S1). From  $^{13}\text{C}$  CP/MAS NMR of HUST-1, the resonance peaks are observed at 127.7 and 138.2 ppm, which are assigned to carbon atoms in the benzene and porphyrin rings, respectively (Fig. S1). The chemical shift at 37.2 ppm signifies the existence of methylene carbon formed by Friedel–Crafts reaction [28]. The FTIR spectra of polymer displays a series of bands around  $1650\text{--}1600\text{ cm}^{-1}$  that were assigned to the  $\text{-C=N-}$  stretching band. The bands around  $1250\text{--}950\text{ cm}^{-1}$  and  $900\text{--}650\text{ cm}^{-1}$  were attributed to benzene skeleton

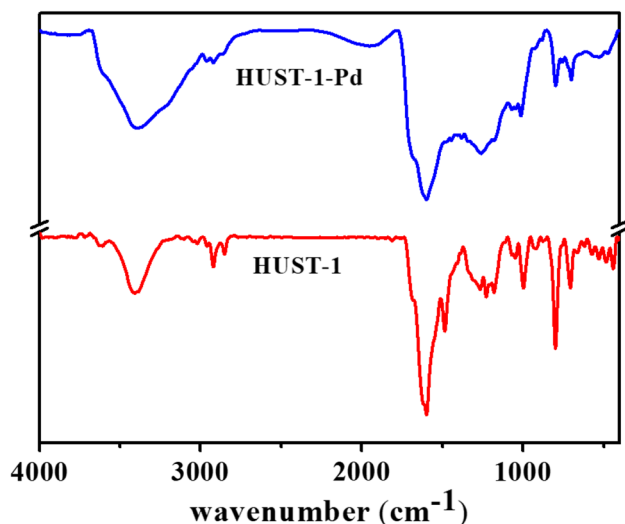


Fig. 1 FT-IR spectra of HUST-1 and HUST-1-Pd

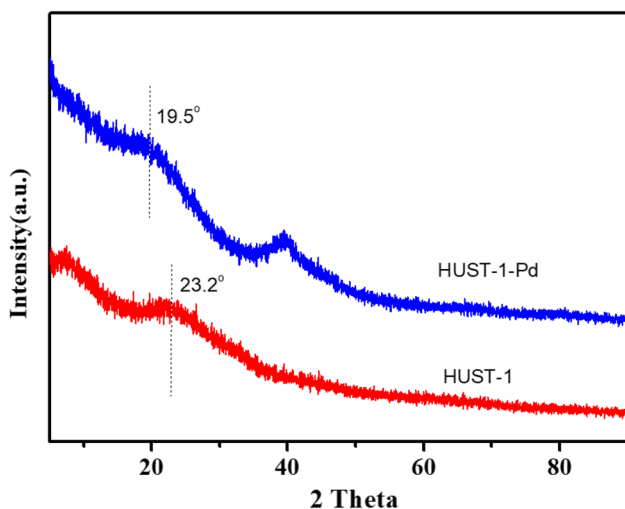


Fig. 2 XRD patterns of highly dispersed HUST-1-Pd and HUST-1

stretching C–H out-of-plane bending and in-plane bending vibrations of the benzene ring, respectively (Fig. 1, red line).

Following the disappearance of C–H stretching vibrations of the aromatic ring, strong C–H stretching vibrations of methylene near 2960–2920  $\text{cm}^{-1}$  can be easily observed, which indicates the formation of methylene linkage (Fig. 1, blue line). Based on above characterizations, the formation of HUST-1 can be confirmed and the chemical structure of HUST-1-Pd remains after incorporation of  $\text{Pd}^{2+}$  and reduction by  $\text{NaBH}_4$ .

The crystal structure of HUST-1-Pd was further studied using power XRD and the typical PXRD pattern is depicted in Fig. 2. In the XRD pattern, one reflection at  $2\theta = 40^\circ$  is ascribable to the (111) plane of an fcc crystal structure of Pd(0) [29]. Using the Scherrer equation, we calculated the crystal size of the Pd NPs to be 4.2 nm.

Beside the peak belonging to fcc-Pd, another widening peak appeared at  $2\theta = 19.5^\circ$  and is attributed to the amorphous structure of the HUST-1 support. However, compared to original peak at  $2\theta = 23.2^\circ$  of HUST-1, the peak migrates about  $4^\circ$ . The results illustrate the support the Pd change in the structure of the metalporphyrin in the polymer. To determine the Pd content of HUST-1-Pd for catalytic applications, atomic absorption spectroscopy (AAS) analysis was performed on the samples and Pd content was found to be 0.73 wt%. This value was used to determine the loading ratio of HUST-1-Pd for catalytic applications.

The porous properties of HUST-1-Pd and HUST-1 were investigated by nitrogen adsorption analysis at 77 K (Fig. 3). According to IUPAC classification [30], HUST-1-Pd and HUST-1 all showed type I nitrogen adsorption isotherms as shown in Fig. 3a. The high uptake at very low pressures (0–0.1 bar) indicates the materials with abundant micropores. With increasing pressure, the nitrogen uptake featured almost no increased, indicating the existence of little external surface area as evidenced by the presence of very small particles. Therefore, HUST-1 has a predominantly microporous structure in its framework. The sharp increase in the nitrogen

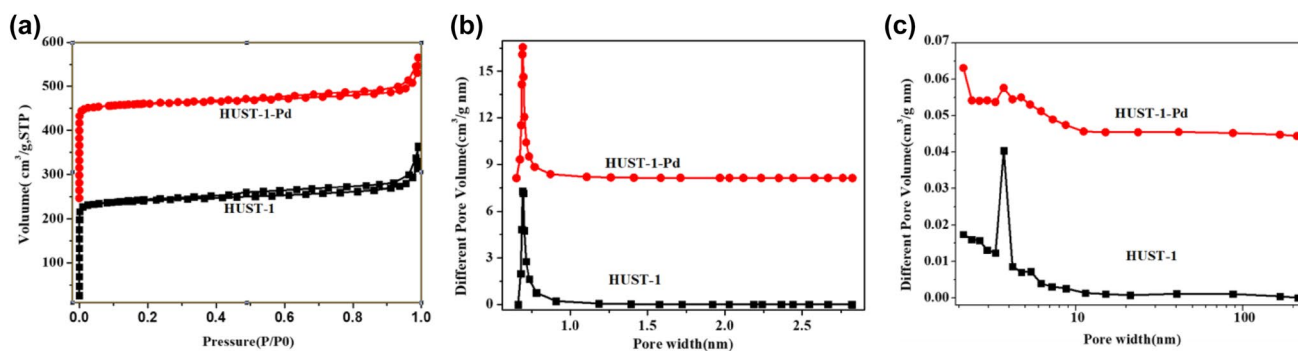
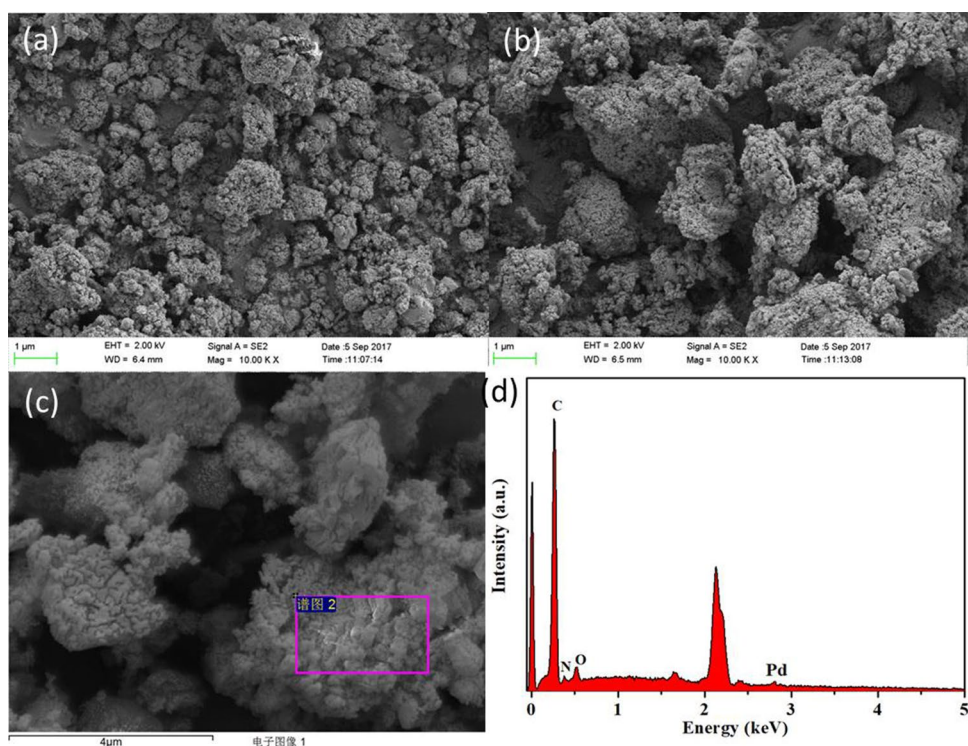


Fig. 3  $\text{N}_2$  adsorption–desorption isotherms and a pore size distribution b, c of HUST-1

**Fig. 4** SEM images of **a** HUST-1, **b** HUST-1-Pd and **c, d** SEM-EDS spectrum from this region of HUST-1-Pd nanocatalyst



uptake at high relative pressure may be attributed in part to interparticulate porosity associated with the meso-structures of the samples. A surface area of 769 and 779  $\text{m}^2\text{g}^{-1}$  were obtained by applying the Brunauer–Emmett–Teller (BET) model for HUST-1-Pd and HUST-1, respectively. The pore size distribution diagram based on the density functional theory (DFT) method in Fig. 3b, c also showed a typical micro/mesoporous nature of the material, which agreed with the shape of nitrogen sorption isotherms and HR-TEM analysis (Fig. 4c). The hierarchical pore structure and abundant Pd of HUST-1-Pd not only enhances the interaction between the pore walls and the substrate, but is also favorable for catalysis processes. The microporous structure could adsorb and catalyze the reactants, and mesopores are beneficial for accelerating the mass transfer of reactants and products. Compared to HUST-1, the mesopores of HUST-1-Pd sometimes disappears due to the palladium particles occupying some pores.

The morphology and porosity of HUST-1 and HUST-1-Pd were recorded by SEM (Fig. 4a, b). The polymers all exhibited irregular particle-aggregated morphologies that are a property of porousness. The results agree with the characterization of the  $\text{N}_2$  adsorption–desorption isotherms test. After cooperation with Pd, the morphology of HUST-1-Pd is almost unchanged (Fig. 4b). SEM–EDX spectrum analyses collected from the selected region of the images given in Fig. 4c, d confirms the presence of Pd and N on the support materials.

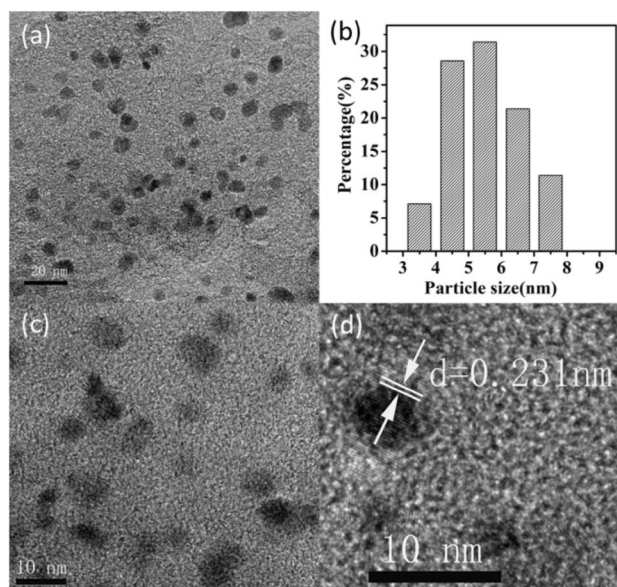


**Fig. 5** TEM images of **a, c** HUST-1-Pd, **b** Pd NPs corresponding size histogram, and **d** HRTEM images of HUST-1-Pd

The TEM images (Fig. 5) indicate that the as synthesized Pd NPs are highly dispersed on the HUST-1 surface and the particle size of Pd NPs was measured and the diameter was found to be about 5.5 nm (Fig. 5b). This size is larger than that measured from XRD, indicating that the as-synthesized NPs are in a polycrystalline structure. A typical distance between crystal fringes of 0.231 nm was calculated from the

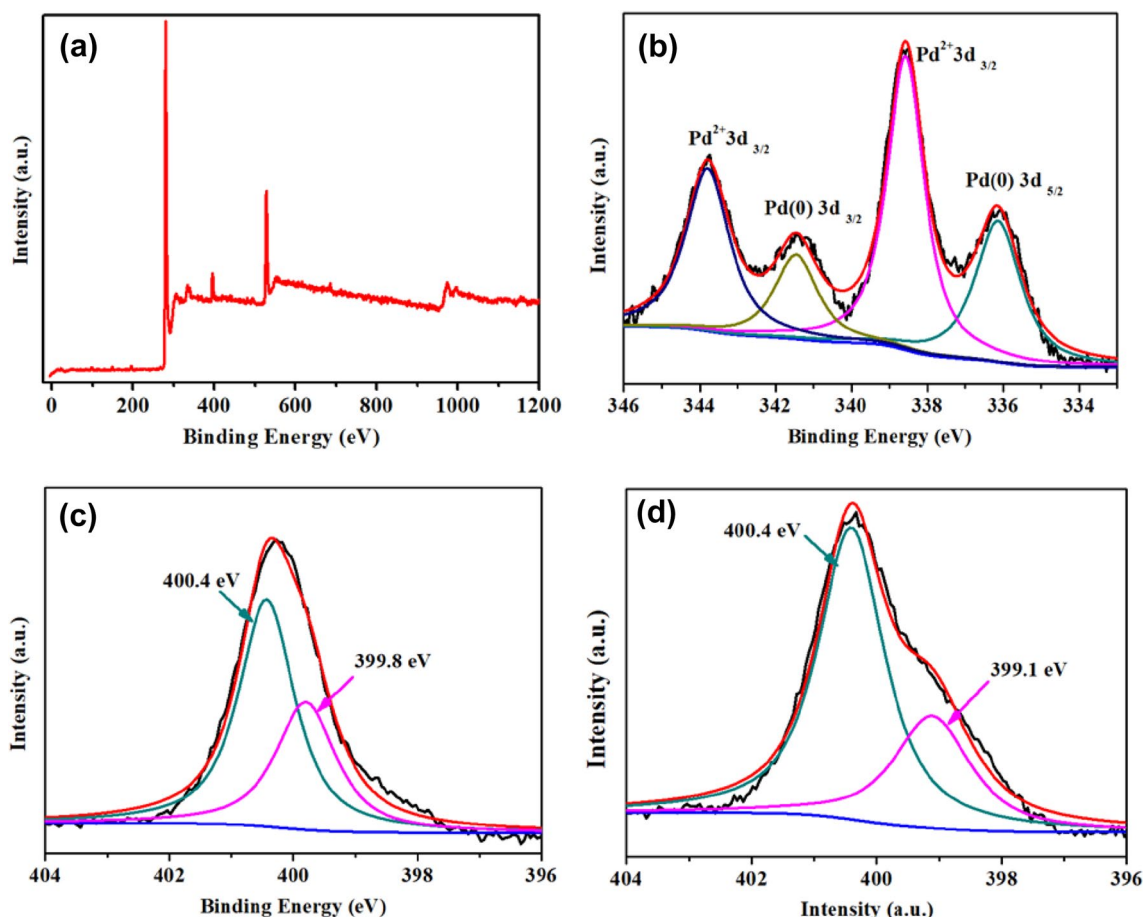


**Fig. 6** XPS analysis of HUST-1 and HUST-1-Pd. **a** Survey scan of HUST-1-Pd; **b** XPS spectra for the Pd 3d species of HUST-1-Pd; **c** high-resolution XPS N1s spectrum of HUST-1-Pd, and **d** high-resolution XPS N1s spectrum of HUST-1

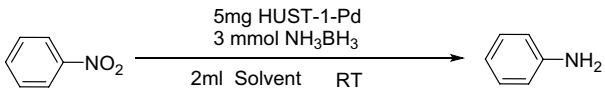
HR-TEM images (Fig. 5d), which is close to the lattice spacing of the (111) planes of the fcc crystal of Pd (0.223 nm) [31], indicating that the Pd(0) has indeed formed.

To gain further insight into the compositions and confirm the oxidation states of the Pd element, X-ray photoelectron spectroscopy (XPS) analysis of HUST-1-Pd was performed (Fig. 6). The XPS survey spectrum in Fig. 6a clearly shows the presence of Pd in HUST-1-Pd, in addition to carbon, oxygen, and nitrogen. As shown in Fig. 6b, the binding energy for Pd(0)  $3d_{3/2}$  and  $3d_{5/2}$  is 341.4 and 336.1 eV, respectively, indicating the presence of zero-valent Pd in HUST-1-Pd. However, the Pd(II) still exists at the binding energy of 343.8 and 338.6 eV. We assume that the Pd(II) species were coordinated to Pd-N<sub>4</sub> and coated by zero-valent Pd so the Pd(II) has been not reduced to Pd(0) [32]. The N1's binding energy of HUST-1 (Fig. 6d) shows two types of nitrogen: one at 399.1 eV for nitrogen in the free-based porphyrin ring, and another at 400.4 eV for the free secondary amine ( $-C=C-NH$ ) [33]. However, HUST-1-Pd exhibits N1 peaks at 400.4 and 399.8 eV (Fig. 6c), which are formed due to the coordination of Pd species with porphyrin rings. Notably, as

observed from the N1s' binding energy of HUST-1-Pd, the absence of the peak at 399.1 eV indicates complete metalation in the porphyrin rings [34]. These results confirm that this bottom-up strategy could facilitate a metalloporphyrin-based porous organic polymer with a higher density active site compared to that of the previously reported porphyrin-based polymers.

## 2.1 Catalytic Properties

Reduction of nitroarenes plays an important role in modern chemistry. To evaluate the catalytic activity of HUST-1-Pd, we chose the tandem reaction of AB dehydrogenation and nitro compound hydrogenation as a model reaction. The reaction was initiated by adding AB to the solution in the flask containing HUST-1-Pd and nitro compounds under magnetic stirring. Thin layer chromatography (TLC) was used to monitor the reaction process and gas chromatography-mass spectrometry (GC-MS) was used to quantify the reaction mixture changes. Nitrobenzene was employed as a model compound in the tandem catalysis over HUST-1-Pd

**Table 1** The effects of solvents in the reaction


Entry	Solvent	Temperature (°C)	Conv. <sup>a</sup> (%)
1	CH <sub>3</sub> OH	25	58.3
2	EtOH	25	70.4
3	H <sub>2</sub> O	25	34.7
4	Ethylene glycol	25	55.7
5	Acetonitrile	25	6.5
6	DMF	25	Trace
7	CH <sub>3</sub> OH/H <sub>2</sub> O	25	> 99.0
8	CH <sub>3</sub> OH/H <sub>2</sub> O	25	81.3
9	EtOH/H <sub>2</sub> O	25	88.9

Reaction conditions: 1 mmol nitrobenzene, 3 mmol NH<sub>3</sub>BH<sub>3</sub>, 5 mg catalysts, 2 mL of MeOH/H<sub>2</sub>O (v:v = 2:3), and room temperature

<sup>a</sup>Catalytic reaction products were analyzed and identified by GC-MS

to explore the optimized reaction parameters. Firstly, we tested the catalytic tandem reactions at room temperature in different solvents including water, methanol, ethanol, and mixtures at various ratios. The reaction optimization data is summarized in Table 1; we observed that the suitable solvent methanol and ethanol resulted in 58.3% and 70.4% yields, respectively (Table 1, entries 1 and 2). In water, ethylene glycol and acetonitrile (Table 1, entries 3–5) show low catalytic activity, but it almost has no yields when DMF is changed as the solvent (Table 1, entry 6). More interestingly, the change in the reaction environment from pure solvent to a water solution had a positive effect on the activity in HUST-1-Pd (Table 1, entries 7–9), a mixture of methanol and water (v:v = 2:3) was found to be the best solvent in the reaction. The reaction proceeded smoothly, and nitrobenzene was converted to aniline very rapidly in as short as 2 min with a real nitrobenzene/Pd molar ratio of 2941 at room temperature. The turnover frequency (TOF) was calculated to be 86,337 h<sup>-1</sup>.

With the optimized conditions, the catalytic results for the tandem reaction with diverse R-NO<sub>2</sub> substrates over HUST-1-Pd are summarized in Table 2. All aromatic or aliphatic nitro compounds investigated were converted into their corresponding primary amines with excellent conversion yields (> 95%) in 5–30 min at room temperature. For example, aliphatic nitro compounds such as nitromethane were reduced in excellent yields in 2 min (Table 2, entry 1) and nitrobenzene was reduced to aniline quantitatively also in 2 min (Table 2, entry 2). The nitro groups in *p*-methyl, *m*-methyl, *o*-methoxy, *m*-chloride, and *p*-chloride-nitrobenzenes

(Table 2, entry 3–7) were also reduced into the related amine products in nearly quantitative conversion yields in 10 min. The results illustrate that slight steric hindrance was tolerated well in the hydrogenation of nitro compounds by HUST-1-Pd. Moreover, several electron-withdrawing and electron-donating nitroarene derivatives have also been successfully reduced by the presented hydrogenation protocol in 30 min, indicating the high substituent tolerance of the presented catalytic transfer hydrogenation protocol (Table 2, entries 8–10). On the other hand, the presented HUST-1-Pd catalyzed transfer hydrogenation showed almost no yields towards the reduction of benzyl chloride on the aromatic ring (Table 2, entry 11).

The stability and reusability of catalysts are of great importance in their practical application. We test the durability of HUST-1-Pd by performing the tandem reaction on nitrobenzene. The catalyst was separated after each reaction and washed with water/methanol for the next round of reactions. After the tenth consecutive use, the catalyst still showed a conversion yield higher than 95% in the same reaction times (Fig. 7), clearly demonstrating the recyclability and reusability of the catalyst. In addition, the Pd NPs retain high dispersion and their sizes were almost retained after 10 runs (Fig. 8), revealing the good confinement effect of HUST-1 based on its porous structure. The AAS results shows that negligible Pd species can be detected in the reacted solution, which reveals that the leaching of active sites almost does not occur during the reaction.

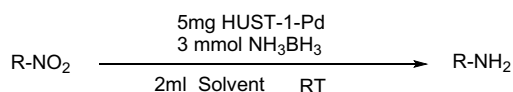
### 3 Conclusion

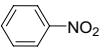
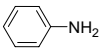
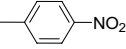
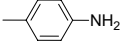
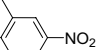
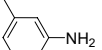
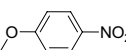
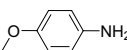
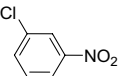
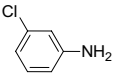
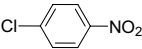
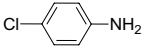
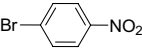
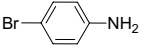
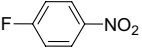
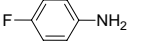
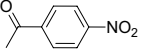
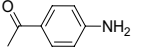
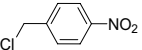
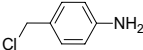
In summary, we have reported a facile route to prepare high-dispersed Pd NP support for porphyrin-based microporous organic polymers. The catalyst was efficient in catalyzing the tandem reaction of the dehydrogenation of AB and hydrogenation of R-NO<sub>2</sub> to produce primary amines (R-NH<sub>2</sub>) at room temperature. In the series of aromatic or aliphatic nitro compounds tested, they were all reduced to the respective primary amines with excellent conversion yields in short reaction times (2–30 min). Furthermore, the catalyst could be easily separated and the yields achieved above 95% after 10 times of reuse. This demonstrates a new strategy to introduce highly-dispersed Pd NPs into porphyrin-based functional polymers through simple steps.

## 4 Experimental Section

### 4.1 Materials

Purchased from Aladdin chemical reagent Corp (Shanghai, China) were 5-, 10-, 15-, 20-teraphenylporphyrin and nitro

**Table 2** HUST-1-Pd catalyzed tandem reaction of various R-NO<sub>2</sub> compounds

Entry	Substrate	Product	Yield <sup>a</sup> (%)	Time (min)	TOF (h <sup>-1</sup> )
1	CH <sub>3</sub> NO <sub>2</sub>	CH <sub>3</sub> NH <sub>2</sub>	99	2	87,209
2			99	2	87,209
3			97	5	33,837
4			95	5	33,140
5			90	10	15,698
6			96	5	33,489
7			90	10	15,698
8			81	30	4709
9			85	30	4942
10			87	30	5058
11			Trace	30	–

Reaction conditions: 1 mmol nitro compound, 3 mmol NH<sub>3</sub>BH<sub>3</sub>, 5 mg of HUST-1-Pd catalyst (0.73 wt% metal content), 2 mL of MeOH:H<sub>2</sub>O (v:v = 2:3), and room temperature

<sup>a</sup>Isolated yield

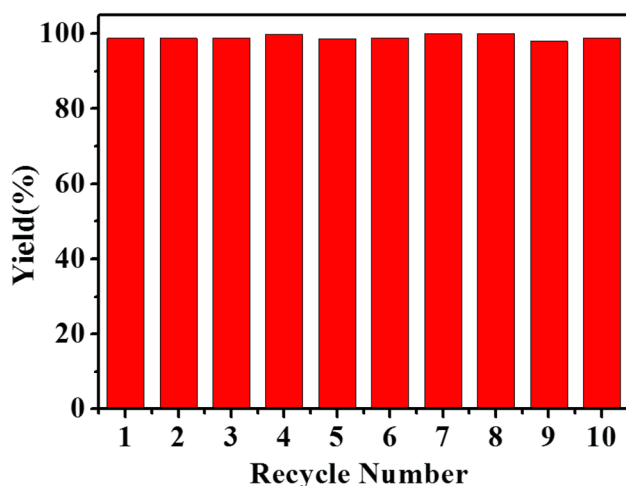


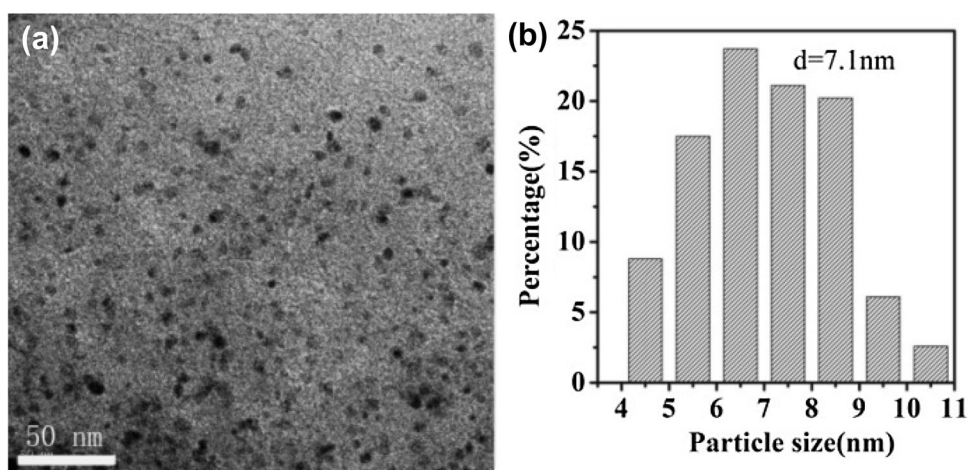
**Fig. 7** The recyclability of HUST-1-Pd for tandem reactions of ammonia borane dehydrogenation and nitrobenzene hydrogenation

compounds; they were used as received. Dichloromethane, ethanol, HCl, anhydrous aluminum chloride, palladium chloride, and NaBH<sub>4</sub> were obtained from Sinopharm Chemical Reagent Co., Ltd. (Shanghai, China) and used as received. Unless otherwise noted, all reagents were obtained from commercial suppliers and used without further purification.

#### 4.2 Preparation of HUST-1 Support Pd NPs

HUST-1 was prepared by using a well-established hyper-crosslinking method; the details of the HUST-1 synthesis procedure can be found in our previous reports [28]. Pd NPs support the HUST-1 by a NaBH<sub>4</sub> reduction method. In the typical process, 10 mg of PdCl<sub>2</sub> is dissolved in 5 mL of water with the addition of 1 mL aqueous HCl (0.1 mol/L) at room temperature with vigorous stirring. Then, 110 mg HUST-1 powder is added to the above mixture, and the

**Fig. 8** TEM images and size distribution of HUST-1-Pd after reuse



slurry is stirred for 12 h and 5 mL  $\text{NaBH}_4$  (0.5 M) solution is mixed with the slurry for 2 h. The catalyst was centrifuged until separation and washed by water, and lastly dried under vacuum at 60 °C for 12 h.

### 4.3 General Procedure for HUST-1-Pd Catalyzed Tandem Dehydrogenation of AB and Hydrogenation of Nitro Compounds

The nitro compounds (1 mmol) and HUST-1-Pd catalyst (5 mg) were mixed in 2 mL of a methanol water solution and stirred for 5 min in a 10 mL glass tube at room temperature. Next, AB (1 mmol) was added to the reaction mixture and the glass tube was closed. The reaction was then continued under vigorous stirring at room temperature for a certain time. The progress of the catalytic reaction was monitored by thin layered chromatography (TLC). Most reactions were completed in a time period of 5–30 min. After completion of the reaction, the catalysts were removed by centrifugation at 5000 rpm and washed three times with water and methanol. Then, the catalysts were allowed to dry for the next use. The solvent was removed by using a rotary evaporator; the crude residue was directly purified by column chromatography on silica gel using acetone. The yields of the reduced compounds were determined by  $^1\text{H}$  NMR with  $\text{CDCl}_3$  as the solvent depending on the product separated.

### 4.4 Characterization

FT-IR spectra were recorded on a Bruker Verter 70 Spectrometer using the KBr disk method. The products of hydrogenation were identified by  $^1\text{H}$  NMR spectra using a Bruker AV400 instrument in  $\text{CDCl}_3$ . Chemical shifts were reported in parts per million (ppm) downfield from tetramethylsilane (TMS). The morphologies were observed with a FEI Sirion 200 field SEM and transmission electron microscope (TEM). Pd content data was obtained using

ASS on a Perkin Elmer AA-800 (USA). The X-ray photoelectron spectroscopy (XPS) data of samples were collected by Krato AXIS-ULTRA DLD-600 photoelectron spectrograph.  $\text{N}_2$  sorption properties and specific surface areas of samples were measured using a Micromeritics ASAP 2020 surface area and porosity analyzer. Before analysis, the samples were degassed at 110 °C for 8 h in a vacuum of  $10^{-5}$  bar. Pore size distribution was calculated by  $\text{N}_2$  adsorption isotherms employing the Tarazona non-local density functional theory (NLDFT) model assuming a slit pore geometry. Total pore volumes were derived from nitrogen sorption isotherms at a relative pressure  $P/P_0 = 0.995$ .

**Acknowledgements** This work was financially supported by the Science and Technology Planning Project of Guangdong Province (2017B030314092), the Fundamental Research Funds of CWNU (17C038) and Meritocracy Research Funds of CWNU (17Y031), Science and Technology Foundation of Sichuan Province (2017JY0015).

### References

1. Yang F, Wang M, Liu W, Yang B, Wang Y, Luo J, Tang Y, Hou L, Li Y, Li Z, Zhang B, Yang W, Li Y (2019) Atomically dispersed Ni as the active site towards selective hydrogenation of nitroarenes. *Green Chem* 21:704
2. Yang Q, Chen YZ, Wang ZU, Xu Q, Jiang HL (2015) One-pot tandem catalysis over Pd@MIL-101: boosting the efficiency of nitro compound hydrogenation by coupling with ammonia borane dehydrogenation. *Chem Commun (Camb)* 51:10419
3. Westerhaus FA, Jagadeesh RV, Wienhöfer G, Pohl M-M, Radnik J, Surkus A-E, Rabeah J, Junge K, Junge H, Nielsen M (2013) Heterogenized cobalt oxide catalysts for nitroarene reduction by pyrolysis of molecularly defined complexes. *Nat Chem* 5:537
4. Yang X, Song K, Tan L, Hussain I, Li T, Tan B (2014) Hollow microporous organic capsules loaded with highly dispersed Pt nanoparticles for catalytic applications. *Macromol Chem Phys* 215:1257



- Luo L, Duan Z, Li H, Kim J, Henkelman G, Crooks RM (2017) Tunability of the adsorbate binding on bimetallic alloy nanoparticles for the optimization of catalytic hydrogenation. *J Am Chem Soc* 139:5538
- Hartmann CE, Jurcik V, Songis O, Cazin CS (2013) Tandem ammonia borane dehydrogenation/alkene hydrogenation mediated by [Pd(NHC)(PR<sub>3</sub>)] (NHC = N-heterocyclic carbene) catalysts. *Chem Commun (Camb)* 49:1005
- Rossin A, Peruzzini M (2016) Ammonia-borane and amine-borane dehydrogenation mediated by complex metal hydrides. *Chem Rev* 116:8848
- Yao Q, Lu Z-H, Yang Y, Chen Y, Chen X, Jiang H-L (2018) Facile synthesis of graphene-supported Ni-CeOx nanocomposites as highly efficient catalysts for hydrolytic dehydrogenation of ammonia borane. *Nano Res* 11:4412
- Yang K, Zhou L, Yu G, Xiong X, Ye M, Li Y, Lu D, Pan Y, Chen M, Zhang L, Gao D, Wang Z, Liu H, Xia Q (2016) Ru nanoparticles supported on MIL-53(Cr, Al) as efficient catalysts for hydrogen generation from hydrolysis of ammonia borane. *Int J Hydrog Energy* 41:6300
- Richard J, Cid SL, Rouquette J, Van Der Lee A, Bernard S, Haines J (2016) Pressure-induced insertion of ammonia borane in the siliceous zeolite, silicalite-1F. *J Phys Chem C* 120:9334
- Shang N, Zhou X, Feng C, Gao S, Wu Q, Wang C (2017) Synergistic catalysis of NiPd nanoparticles supported on biomass-derived carbon spheres for hydrogen production from ammonia borane at room temperature. *Int J Hydrog Energy* 42:5733
- Wen M, Cui Y, Kuwahara Y, Mori K, Yamashita H (2016) Non-noble-metal nanoparticle supported on metal-organic framework as an efficient and durable catalyst for promoting H<sub>2</sub> production from ammonia borane under visible light irradiation. *ACS Appl Mater Interfaces* 8:21278
- Ma X, Zhou YX, Liu H, Li Y, Jiang HL (2016) A MOF-derived Co-CoO@N-doped porous carbon for efficient tandem catalysis: dehydrogenation of ammonia borane and hydrogenation of nitro compounds. *Chem Commun (Camb)* 52:7719
- Zhou Y-H, Yang Q, Chen Y-Z, Jiang H-L (2017) Low-cost CuNi@MIL-101 as an excellent catalyst toward cascade reaction: integration of ammonia borane dehydrogenation with nitroarene hydrogenation. *Chem Commun* 53:12361
- Altintas C, Erucar I, Keskin S (2018) High-throughput computational screening of the metal organic framework database for CH<sub>4</sub>/H<sub>2</sub> separations. *ACS Appl Mater Interfaces* 10:3668
- Luo S, Zhang Q, Zhang Y, Weaver KP, Phillip WA, Guo R (2018) Facile synthesis of a pentiptycene-based highly microporous organic polymer for gas storage and water treatment. *ACS Appl Mater Interfaces* 10:15174
- Gu S, Guo J, Huang Q, He J, Fu Y, Kuang G, Pan C, Yu G (2017) 1,3,5-Triazine-based microporous polymers with tunable porosities for CO<sub>2</sub> capture and fluorescent sensing. *Macromolecules* 50:8512
- Bai Y, Chen BWJ, Peng G, Mavrikakis M (2018) Density functional theory study of thermodynamic and kinetic isotope effects of H<sub>2</sub>/D<sub>2</sub> dissociative adsorption on transition metals. *Catal Sci Technol* 8:3321
- Tang C, Zou Z, Fu Y, Song K (2018) Highly dispersed DPPF locked in knitting hyper-crosslinked polymers as efficient and recyclable catalyst. *ChemistrySelect* 3:5987
- Su J, Chen J-S (2017) Synthetic porous materials applied in hydrogenation reactions. *Microporous Mesoporous Mater* 237:246
- Chen X, Shen K, Ding D, Chen J, Fan T, Wu R, Li Y (2018) Solvent-driven selectivity control to either anilines or dicyclohexylamines in hydrogenation of nitroarenes over a bifunctional Pd/MIL-101 catalyst. *ACS Catal* 8:10641
- Bera R, Mondal S, Das N (2018) Triptycene based microporous polymers (TMPs): efficient small gas (H<sub>2</sub> and CO<sub>2</sub>) storage and high CO<sub>2</sub>/N<sub>2</sub> selectivity. *Microporous Mesoporous Mater* 257:253
- Wang M, Ye C, Xu M, Bao S (2018) MoP nanoparticles with a P-rich outermost atomic layer embedded in N-doped porous carbon nanofibers: self-supported electrodes for efficient hydrogen generation. *Nano Res* 11:4728
- Eghbali P, Nişancı B, Metin Ö (2018) Graphene hydrogel supported palladium nanoparticles as an efficient and reusable heterogeneous catalysts in the transfer hydrogenation of nitroarenes using ammonia borane as a hydrogen source. *Pure Appl Chem* 90:327
- Zhu W, Wang X, Li T, Shen R, Hao SJ, Li Y, Wang Q, Li Z, Gu ZG (2018) Porphyrin-based porous polyimide polymer/Pd nanoparticle composites as efficient catalysts for Suzuki-Miyaura coupling reactions. *Polym Chem* 9:1430
- Kumar S, Thorat KG, Lee WZ, Ravikanth M (2018) Synthesis, structural, spectral, and electrochemical studies of selenabenzoporphyrin and its Pd(II) complex. *Inorg Chem* 57:8956
- Fu Y-F, Song K-P, Zou Z-J, Li M-Q (2018) External cross-linked sulfonate-functionalized N-heterocyclic carbenes: an efficient and recyclable catalyst for Suzuki-Miyaura reactions in water. *Transit Met Chem* 43:665
- Wang S, Song K, Zhang C, Yu S, Tao L, Tan B (2017) A novel metalporphyrin-based microporous organic polymer with high CO<sub>2</sub> uptake and efficient chemical conversion of CO<sub>2</sub> under ambient conditions. *J Mater Chem A* 5:1509
- Karataş Y, Gülcan M, Celebi M, Zahmakiran M (2017) Pd(0) nanoparticles decorated on graphene nanosheets (GNS): synthesis, definition and testing of the catalytic performance in the methanolysis of ammonia borane at room conditions. *ChemistrySelect* 2:9628
- Sheng X, Guo H, Qin Y, Wang X, Wang F (2015) A novel metalloporphyrin-based conjugated microporous polymer for capture and conversion of CO<sub>2</sub>. *RSC Adv* 5:31664
- Gulcan M, Zahmakiran M, Özkar S (2014) Palladium(0) nanoparticles supported on metal organic framework as highly active and reusable nanocatalyst in dehydrogenation of dimethylamineborane. *Appl Catal B* 147:394
- Veisi H, Najafi S, Hemmati S (2018) Pd(II)/Pd(0) anchored to magnetic nanoparticles (Fe<sub>3</sub>O<sub>4</sub>) modified with biguanidine-chitosan polymer as a novel nanocatalyst for Suzuki-Miyaura coupling reactions. *Int J Biol Macromol* 113:186
- Chandra S, Kundu T, Dey K, Addicoat M, Heine T, Banerjee R (2016) Interplaying intrinsic and extrinsic proton conductivities in covalent organic frameworks. *Chem Mater* 28:1489
- Ding ZD, Zhu W, Li T, Shen R, Li Y, Li Z, Ren X, Gu ZG (2017) A metalloporphyrin-based porous organic polymer as an efficient catalyst for the catalytic oxidation of olefins and arylalkanes. *Dalton Trans* 46:11372

**Publisher's Note** Springer Nature remains neutral with regard to jurisdictional claims in published maps and institutional affiliations.

## Affiliations

Zhijuan Zou<sup>1</sup> · Yaya Jiang<sup>1</sup> · Kunpeng Song<sup>1,2</sup>

✉ Kunpeng Song  
song19880405@126.com

<sup>1</sup> Chemical Synthesis and Pollution Control Key Laboratory of Sichuan Province, College of Chemistry and Chemical Engineering, China West Normal University, Shida Road 1#, Nanchong 637009, China

<sup>2</sup> Institute of Synthesis and Application of Functional Materials, China West Normal University, Nanchong 637009, China